Analysis of Cluster Engine Instabilities and Plume Characteristics

a project presented to

The Faculty of the Department of Aerospace Engineering

San José State University

in partial fulfillment of the requirements for the degree

Master of Science in Aerospace Engineering

by

Atharva Sawant

May 2025

approved by

Dr. Periklis Papadopoulos
Faculty Advisor

ABSTRACT

Analysis of Cluster Engine Instabilities and Plume Characteristics

Atharva Sawant

In modern launch vehicles, the use of clustered engine configurations has become second nature to boost thrust, improve reliability, and reduce development costs through modularity and faster production. However, these configurations come with many caveats due to the complex interactions between their exhaust plumes, especially at high altitudes. This project investigates the base flow region of multi-nozzle cluster rocket engines in terms of turbulence characteristics and thermal environment using CFD simulations.

Various nozzle configurations, like 3,4,5, and 7 nozzle setups, were simulated at two different altitudes using species transport, turbulence modeling (SST k-ω), along with discrete ordinates radiation. Through the findings, it is clear that base heating increases with altitude due to the underexpansion of plumes. Among the selected configurations, the circular nozzle configurations showed drastic updraft flows due to the cavity between the nozzles, thus heating the centre of the base plate, while the staggered configurations were able to reduce the recirculation due to the central nozzle.

Many successful rockets, like the SpaceX Falcon 9 or the Saturn V S-1C, use non-symmetric layouts to manage the thermal loads in the base region. This study provides insight into the influence of nozzle count, placement, and altitude on the thermal characteristics of the base region and outlines a way of optimizing the multi-engine systems to minimize thermal load on structures.

ACKNOWLEDGMENTS

I would sincerely like to thank Dr. Periklis Papadopoulos, my faculty advisor and mentor, for his guidance, encouragement, and most importantly, his patience throughout this project. Despite missed deadlines and delays on my part, he remained supportive and understanding, which gave me the space to eventually complete this work.

To my parents, thank you for standing by me during this journey. Your support has been invaluable. I would also like to thank Janhvi, whose constant encouragement and patience helped me push through the most challenging moments.

A special thanks to Dr. Yawo Ezunkpe and Igor Eramov for their help in the CFD Setup, guidance, and insights that helped me understand the setups better.

TABLE OF CONTENTS

Introduction **1**
1. Literature Review **2**
1.1 Multi-Engine Instabilities and Flow Interactions 2
1.2 Plume Characterization of Multi-Engine Rocket 4
1.3 Impact of Asynchronous Startups 5
1.4 Dynamics and Computation of Multi-Engine Systems 7
2. Mathematical Model **9**
2.1 Governing Equations: 9
2.2 Turbulence Modeling: 10
3. Computational Setup **14**
3.1 Finite Volume Method: 14
3.2 Accuracy and Errors: 14
3.3 Assumptions: 15
3.4 Stability Considerations: 15
3.5 Implementation of CAD Software: 15
3.6 Meshing: 18
3.7 NASA CEA: 21
3.8 Ansys Fluent Setup: 22
4. Results and Discussions **23**
4.1 Overview of Cases and Metrics: 23
4.2 Effects of Altitude on Base Heating: 24
4.3 Effects of Altitude on Base Heating: 25
4.4 Discussions: 28
5. Conclusions and Future Work **29**
References **30**
Appendix A: NASA CEARUN Input File **32**
Appendix B: NASA CEARUN Output File **33**

LIST OF FIGURES

Figure 1.1 - Flow dynamic structure [3]..... 3
A. Side cross-section B. Top-down sectional view.....3
Figure 1.2 - Simple cluster rocket engine configurations[5]..... 3
Figure 1.3- Moderately under-expanded plumes and flow fields for a 4-engine clustered rocket engine.[8]..... 5
Table 1.1- Flow interactions and their impacts..... 5
Figure 1.4- LOX flow rates [10]..... 6
Figure 1.5- Heat flux on rocket base plate[22]..... 8
Table 2.1- Comparison between k- and k- models..... 12
Table 3.1- Geometry and Configuration of the Engine.....16
Figure 3.1- Laval Nozzle..... 16
Table 3.2- Co-ordinate for Laval Nozzle..... 16
Figure 3.2- Linear Nozzles..... 17
Figure 3.3- Circular Nozzles.....18
Figure 3.4- Circular Nozzles.....18
Figure 3.5- ANSYS Parameters.....20
A. Refined mesh using face meshing B. Inflation layers near the boundary.....21
Table 3.3- CEARUN Inputs..... 21
Table 4.1- CEARUN Inputs..... 23
Figure 4.1- 4-Nozzle Configuration Mach Number Contours..... 25
Figure 4.2- Temperature contours for nozzle configuration at low and high altitudes..... 27
Table 4.2- Results Summary..... 27

SYMBOLS

Symbol	**Definition**	**Units (SI)**
ν	Kinematic Viscosity	m^2/s
l	Characteristic Length	m
T	Temperature	K
k_{th}	Thermal Conductivity	$W/m \cdot K$
U	Mean Velocity Component	m/s
S	Strain Rate Tensor	1/s
p	Pressure	Pa
f	External Body Forces	N
E	Total energy per unit volume	J/m^3
e	Internal Energy	J/kg
I	Turbulence Intensity	
L	Length Scale	
Greek Symbol		
ρ	Density	kg/m^3
ν	Velocity Vector	m/s
τ	Viscous Stress Tensor	Pa
μ	Dynamic Viscosity	Pa.s
Φ	Viscous Dissipation	W/m^3
k	Turbulent Kinetic Energy	m^2/s^2

ω	Specific Dissipation Rate	1/s
τ_{RE}	Reynolds Stress Tensor	kg/ms^2
β	Dissipation Coeffient	-
α	Production Coefficient	-
σ	Diffusion Coefficient	-
σ_d	Corrective Factor	-
f_β	Beta Correction Factor	-
χ_ω	Parameter quantifying the effects of rotation and strain on turbulence	-
Ω	Rotation Rate Tensor	-
Subscripts		
$()_{i,j,k}$	Indices for Spatial Directions on the Cartesian Plane	
$()_t$	Turbulence	
$()_c$	Characteristic	
$()_\infty$	Free Stream Condition	
Acronyms		
CFD	Computational Fluid Dynamics	
RANS	Reynolds Averaged Navier-Stokes	
SLS	Space Launch System	

DC-X	Delta Clipper Experimental	
SU k-ω	Shock Unsteadiness k-ω Model	
DNS	Direct Numerical Simulation	
LOX	Liquid Oxygen	
k-ϵ	Turbulence Kinetic Energy (k) - Turbulence Dissipation Rate (ϵ) Model	
k-ω	Turbulence Kinetic Energy (k) - Specific Dissipation Rate (ω) Model	
LRE	Liquid Rocket Engines	
SA	Spalart Allmaras	
RKE	Realizable k-ε	
RNG	Renormalization Group k-ε	
BSL	Baseline k-ω	
SST	Shear-Stress Transport k-ω	
LES	Large Eddy Simulation	

Introduction

Multi-engine systems are widely used in modern space vehicles to increase performance and provide redundancy, significantly increasing the complexity, points of failure, and instability risks. These risks become particularly important to assess in the context of asynchronous startups and complex interactions between engine plumes, which can cause reverse flow, base heating, and misbalanced thrust. Numerous studies show that multi-engine interactions and instabilities have critical impacts on performance. Under expanded supersonic plumes, shockwaves, and turbulent shear layers are a few phenomena that can lead to pressure drops, cavitation breakdowns, and severe transient processes.

This project focuses on analyzing these multi-engine instabilities and plume characteristics in clustered rocket engines by studying computational fluid dynamics (CFD) simulations and Reynolds Averaged Navier-Stokes equations (RANS). This project would emphasize interactions between multiple exhaust plumes, reverse flow phenomenon, and turbulent shock interactions to understand the impact of various configurations used in modern rockets like Falcon-9, SLS Core Block, and Saturn V (S-1C).

1. Literature Review

1.1 Multi-Engine Instabilities and Flow Interactions

The study of cluster engines has shown that multiple plumes can lead to instabilities. The interactions between the plumes result in reverse flow interactions that lead to shocks, expansion waves, and turbulent flow, severely affecting rocket performance. The shock-unsteadiness model (SU k-ω) proves effective in capturing shock-turbulence interactions, validated by Wilcox 1988 k-ω[1].

During the study of launch vehicles, it is important to understand the transition from continuum to free molecular flow. To understand this, we need to consider the Knudsen Number and density of the atmosphere, as the mean path of the molecules is larger than the nozzle length. Fluid Flow can be characterized as:

- Stokes
- Laminar
- Transition
- Full Turbulence

The rocket exhaust flow (plume core) is fully turbulent as it is supersonic in the gas regime, while the flow is subsonic and laminar near the boundary[2] [3]. The results demonstrated that the various base flows and their interactions create unsteady and complex which can be difficult to assess using analytical methods.

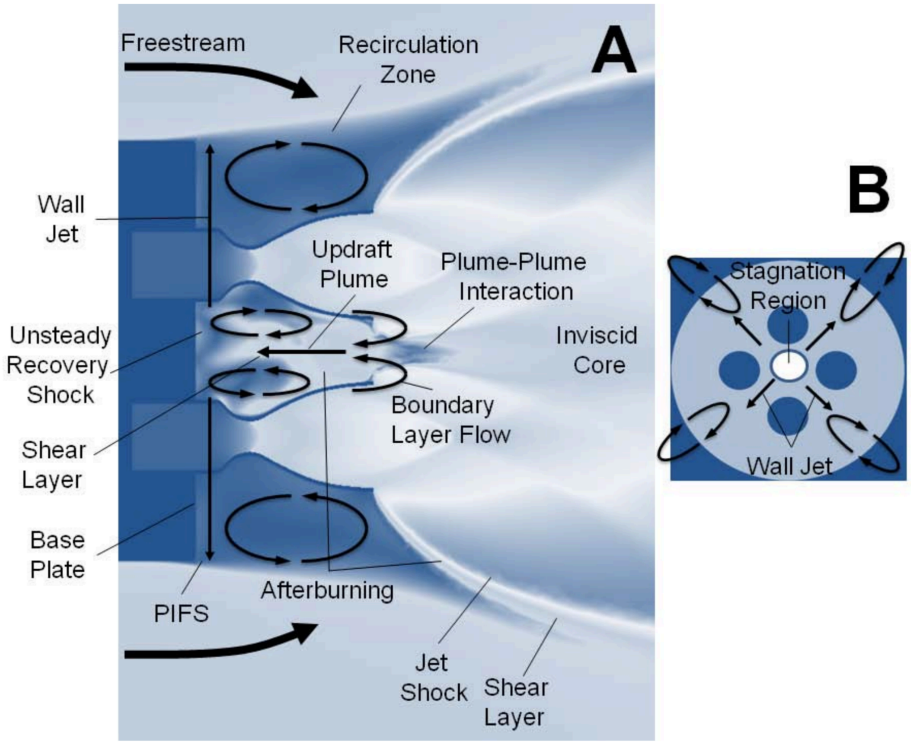

Figure 1.1 - Flow dynamic structure [3]

A. Side cross-section *B. Top-down sectional view*

Similarly, the boundary layer expands at the base shoulder, separating as a free-shear layer and enclosing the low-pressure base flow region with embedded subsonic vortices. During the medium altitude case with moderately under-expanded plumes, the exhaust gases expand rapidly at the exit of the nozzle. Thus, generating an expansion fan and a jet shear layer, forming an external shock at the nozzle-exit plane. As a result of the impingement of these supersonic exhaust gases, we find trailing shocks and an updraft plume due to the high-pressure gradient[4].

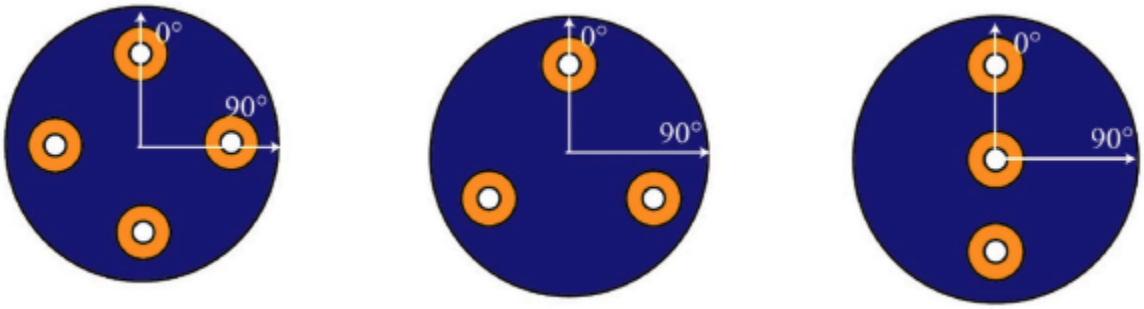

Figure 1.2 - Simple cluster rocket engine configurations[5]

The recirculation region for different configurations is usually different. In a few cases, the recirculation is extreme, while in others it is significant but is reduced as

the altitude increases. The reverse flow that causes this high-temperature recirculation at the baseplate is more in 4-engine configurations, as seen on the SLS and DC-X. This recirculation aggravates the heating of the baseplate. In other configuration,s like the 3-nozzle 180°, with radial layou,t has 62% less heat flux than the 4-nozzle configuration[5]. Similar to this, the intra-nozzle spacing has a significant impact on the plume impingement shock location and shear layer[6].

During the same study, it was observed that while the descent stage for reusable rockets such as Falcon-9 has a similar configuration to the 3-nozzle 180°, the increasing ambient pressure amplifies the convective heating at the base plate and sidewalls. This occurs at around 33km - 22km, a similar trend is observed during the experiments done on launch vehicles using 3 and 4 nozzle configurations.

1.2 Plume Characterization of Multi-Engine Rocket

The clustering of rockets is beneficial as engine development of several sizes can be avoided, resulting in the use of off-shelf engines to meet the requirements of the mission. However, because of the base heating effects caused by the jet interaction, it becomes necessary to add a heat shield to the base components. Thus, defeating the entire purpose of the performance gained due to lightweight engines. Considering the gas dynamics of shockwaves, expansion fans, and their impingement, the following diagram shows the schematics of multi-jet interactions in flowfields for moderately under-expanded plumes[7].

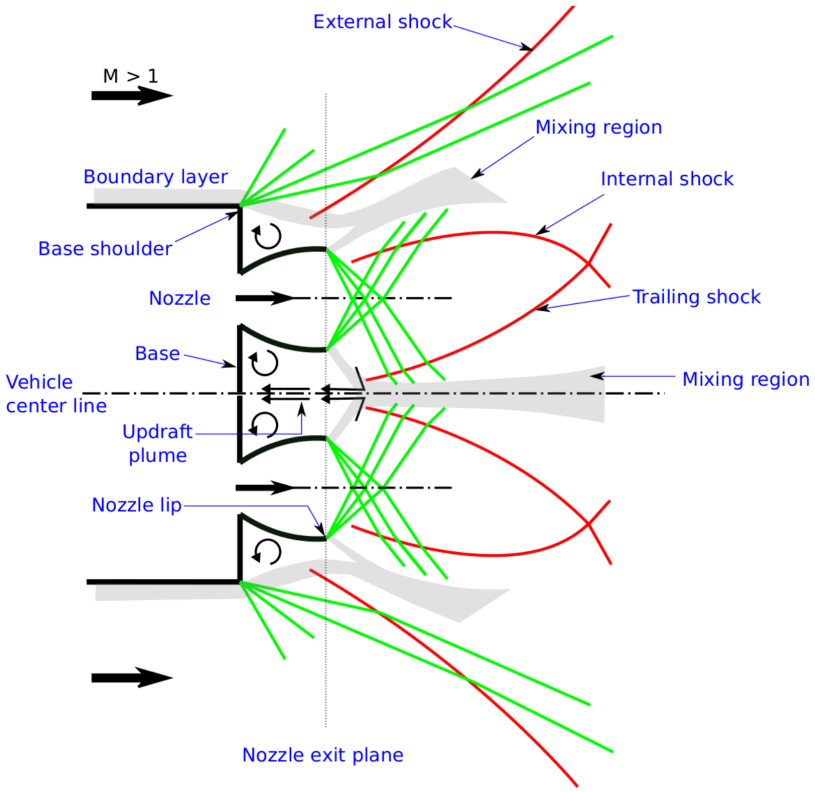

Figure 1.3- Moderately under-expanded plumes and flow fields for a 4-engine clustered rocket engine[8].

Based on Figure 1.3, we can draw the following conclusions:

Table 1.1- Flow interactions and their impacts

Phenomenon	Description	Impact
Viscous and Turbulent Effects	Determine shear layer thickness and reversed flow strength	Influence base pressure and heat transfer rates
Shock-Turbulence Interaction	Occurs when shear layers and shock waves collide.	Amplifies turbulent fluctuations, affecting inflection point location and recirculation region size.
Inflection Point	A region where shear layers converge.	Turbulence amplification at the trailing shock influences reversed flow turbulence.
Updraft Flow	Subject to viscous and turbulent dissipation.	Determines gas pressure and temperature at the base stagnation point.
Shock-Unsteadiness k-ω	Model based on shock-turbulence physics, validated against DNS data.	Accurately amplifies turbulence kinetic energy at shock waves.

Mach distribution of the plume field suggests that as the flight altitude rises, the expansion angle of the jet increases, and the interaction between the jets forms a collision zone. The collision zone's upper boundary remains close to the rocket's base plate. As the jet collides, it gradually generates a gas flow toward the baseplate, causing a process called gas reflux. With increasing height, the incoming pressure rapidly declines, weakening the jet's compression and further intensifying its expansion.

1.3 Impact of Asynchronous Startups

Due to the complexity of cluster rocket engines, it is important to understand the effect of various components and disturbances acting on the parts of the engine. The asynchronous startup of engines in a cluster can cause various issues, such as thrust

misbalance, pump cavitation, pogo oscillations, and stress on the base plate of the engine. Due to the asynchronous nature of these engine startups, it becomes difficult to control the transient dips in Fuel and Oxidizer flow rates and pressures. Based on the simulation results, it becomes evident that during a substantial period of engine startup, pressure fluctuations (up to the LOX pressure of saturated vapor) can occur. These fluctuations can lead to pump cavitation breakdowns in one or more liquid propellant rocket engines from the cluster. These breakdowns can disrupt the entire propulsion system and potentially fail the rocket launch[9].

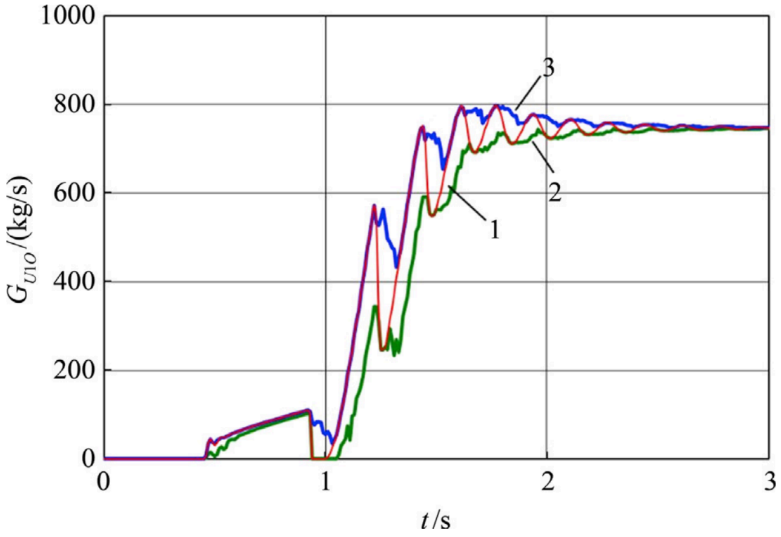

Figure 1.4- LOX flow rates [10]

The diagram above shows the dips and overshoots in the feedlines during the transient states, as the engine startup is asynchronous.

In a multi-engine system, the interaction between individual liquid rocket engines (LREs) and a combination of their internal and external influences can result in hazardous thrust discrepancies. These inconsistencies can affect not only the performance of each engine but also the propulsion system as a whole during startup. At best, such anomalies may cause the launch vehicle to deviate significantly from its intended trajectory during the initial flight phase. In the worst-case scenario, these issues could lead to a complete failure of the launch[10].

Studies done on the Cyclone 4-M rocket show that the mathematical model used to predict and simulate the launch is reliable in accommodating the effects of the spread of internal and external forces on the transient processes in a multi-engine system. This system took into account all the significant low-frequency dynamic processes in the sustainer engine along with the vast internal factors affecting it. These models are based on dozens and hundreds of differential and algebraic equations[11].

Along with the asynchronous start-ups, the pogo oscillations developed during the launch of the vehicle can also affect the performance and stability of the launch vehicle. Thus, mitigating the risk of POGO instability also plays an important role in minimizing asynchronous startups. Using the Nyquist criterion, it is possible to find unstable modes and design the launch vehicle accordingly. Installing POGO suppressors with satisfactory stability margins can ensure POGO stability not only by the nominal values of operating conditions but also by various combinations of limiting values[12] [13].

1.4 Dynamics and Computation of Multi-Engine Systems

The complex nature of the cluster engine rocket configuration makes it difficult to model accurately for simulations. While the experimental setup of these rockets has a steep setup cost, mathematical setups make it much more accessible and economical for researchers to explore the field. The risk involved in testing launch vehicles can be expensive and time-consuming, hindering the primary goal of cluster engines over massive first-stage engines. The intricacies involved in integrating and testing the cluster can be simplified through CFD modeling of the launch vehicle.

Over the years, many researchers have tried to find a way to accurately predict the base heating in clustered rocket engines, as it is crucial for building reliable rockets. The high temperature and complex flow interactions between the impinged plumes make it very difficult to make a model that can be used reliably. Various RANS turbulence models to simulate base heating have been studied over the years[14].

The five models:

- Spalart Allmaras (SA) [15]
- Realizable $k - \epsilon$ (RKE) [16]
- RNG $k - \epsilon$ [17]
- Baseline $k - \omega$ (BSL) [18]
- Shear-Stress Transport $k - \omega$ (SST)

Out of all the model,s SST was best in predicting the central heat flux, closest to the experimental data. The BSL model excelled at predicting the reverse flow. The shear-stress model offers a significant increase in accuracy over the previous turbulence models. It stands out among the two-equation models for its proven ability to reliably predict pressure-induced separation and the resulting interaction between viscous and inviscid flow regions, which is important for the plume impingement characteristics[18] [19].

For simulating the multi-jet interaction flow field, the three-dimensional Reynolds-averaged Navier-Stokes (RANS) equation with Favre decomposition of the variables can be employed [20]. The RANS models do not account for the unsteady motion of the shockwave during these interactions, Sinha et al. [Phys. Fluids, Vol. 15,

No. 8 (2003)] propose a shock-unsteadiness correction that significantly improves turbulence prediction across a normal shock in a uniform mean flow [21]. These improvements can be validated through the CFD code used in past simulations.

Another way to study the base flow regimes in multi-nozzle configurations is by using a hybrid RAN/LES approach, focusing on the thermal environment characteristics affected by the plume impingement. As the number of engines increases, the plume interactions become stronger, significantly increasing the resulting heat. For instance, a four-engine configuration showed a 34.75% and 56.52% increase in the maximum pressure coefficient compared to the three-engine and two-engine configurations, respectively.

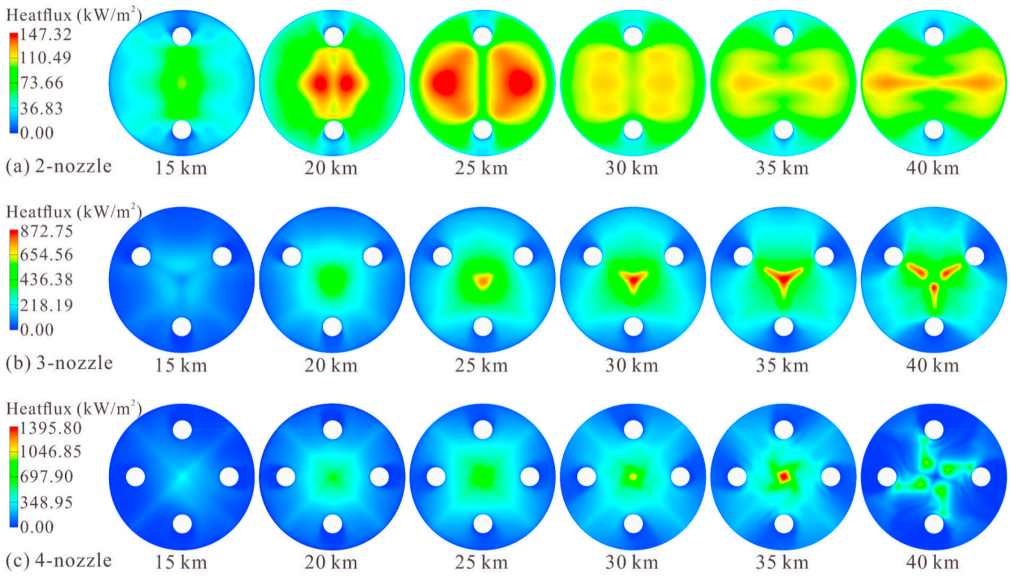

Figure 1.5- Heat flux on rocket base plate[22]

The figure shows the heat flux contours during the launch of 3 engine configurations varying as the altitude of the vehicle increases. Increasing the number of engines increases the heat generated. The heating rate increases initially till about 30-35km and then decreases as the vehicle reaches around 40km altitude [22].

2. Mathematical Model

The mathematical model provides the basics of analyzing fluid dynamics, thermodynamics, and turbulence effects of a clustered rocket engine. The equations governing the characteristics are discussed below.

2.1 Governing Equations:

2. 1. 1 Navier-Stokes Equations

The Navier-Stokes equation is a special continuity equation, derived from the conservation of mass, momentum, and energy [20].

1. Conservation of Mass:

$$\frac{\partial \rho}{\partial t} + \nabla \cdot (\rho v) = 0 \tag{2.1}$$

Where,

- ρ : $Density\ \left(kg/m^3\right)$.
- v : $Velocity\ Vector\ (m/s)$.

2. Conservation of Momentum:

$$\frac{\partial (\rho v)}{\partial t} + \nabla \cdot (\rho v \otimes v) = -\nabla p + \nabla \cdot \tau + f \tag{2.2}$$

Where,

- p : $Pressure\ (Pa)$.
- τ : $Viscous\ Stress\ Tensor$:

$$\tau = \mu\left(\nabla v + (\nabla v)^T\right) - \frac{2}{3}\mu(\nabla \cdot v)I \tag{2.3}$$

- f : $External\ Body\ Forces$.
- μ : $Dynamic\ Viscosity\ (Pa.s)$.

3. Conservation of Energy:

$$\frac{\partial E}{\partial t} + \nabla \cdot [(E + p)v] = \nabla \cdot (k \nabla T) + \Phi \tag{2.4}$$

Where,

- E: Total energy per unit volume:

$$E = \rho\left(e + \frac{|v|^2}{2}\right) \tag{2.5}$$

- $e : Internal\ Energy\ (J/kg)$.
- $|v|^2/2 :\ Kinetic\ Energy$.
- $k :\ Thermal\ conductivity\ (W/m \cdot K)$.
- $T :\ Temperature\ (K)$.
- $\Phi :\ Viscous\ Dissipation$.

$$\Phi = \tau : \nabla v \tag{2.6}$$

2. 1. 2 Boundary Layer Equations:

The analysis can be done using the incompressible boundary-layer equations, for conservation of mass and momentum, as they are sufficient for establishing the form of expansions.

1. Continuity Equation:

$$\frac{\partial u}{\partial x} + \frac{\partial v}{\partial y} = 0 \tag{2.7}$$

2. Momentum Equation:

$$\rho\left(u\frac{\partial u}{\partial x} + v\frac{\partial v}{\partial y}\right) = -\frac{\partial p}{\partial x} + \mu\frac{\partial^2 u}{\partial y^2} \tag{2.8}$$

2.2 Turbulence Modeling:

2. 2. 1 $k - \omega$ Model:

Considering the $k - \omega$ model, we can refer to the equation defining the turbulence model as follows:

1. Kinematic Eddy Viscosity:

$$v_T = \frac{k}{\tilde{\omega}}, \qquad \tilde{\omega} = max\left\{\omega,\ C_{lim}\sqrt{\frac{2S_{ij}S_{ij}}{\beta^*}}\right\}, \qquad C_{lim} = \frac{7}{8} \tag{2.9}$$

2. Turbulence Kinetic Energy:

$$\frac{\partial k}{\partial t} + U_j\frac{\partial k}{\partial x_j} = \tau_{ij}\frac{\partial U_i}{\partial x_j} - \beta^* \cdot k\omega + \frac{\partial}{\partial x_j}\left[\left(v + \sigma^* \cdot \frac{k}{\omega}\right)\frac{\partial k}{\partial x_j}\right] \tag{2.10}$$

3. Specific Dissipation Rate:

$$\frac{\partial \omega}{\partial t} + U_j\frac{\partial \omega}{\partial x_j} = \alpha\frac{\omega}{k}\tau_{ij}\frac{\partial U_i}{\partial x_j} - \beta\omega^2 + \frac{\sigma d}{\omega}\frac{\partial k}{\partial x_j}\frac{\partial \omega}{\partial x_j}\left[\left(v + \sigma\frac{k}{\omega}\right)\frac{\partial \omega}{\partial x_j}\right] \tag{2.11}$$

4. Closure Coefficients and Auxiliary Relations:

$$\alpha = \frac{13}{25}, \beta = \beta_0 f_\beta, \beta^* = \frac{9}{100}, \sigma = \frac{1}{2}, \sigma^* = \frac{3}{5}, \sigma_{do} = \frac{1}{8} \tag{2.12}$$

$$\sigma_d = \begin{cases} 0, & \frac{\partial k}{\partial x_j}\frac{\partial \omega}{\partial x_j} \le 0 \\ \sigma_{do}, & \frac{\partial k}{\partial x_j}\frac{\partial \omega}{\partial x_j} > 0 \end{cases} \tag{2.13}$$

$$\beta_0 = 0.0708, \tag{2.14}$$

$$f_\beta = \frac{1+85\chi_\omega}{1+100\chi_\omega}, \tag{2.15}$$

$$\chi_\omega \equiv \left| \frac{\Omega_{ij}\Omega_{jk}S_{ki}}{(\beta^*\omega)^3} \right| \tag{2.16}$$

$$\epsilon = \beta^* \omega k \tag{2.17}$$

$$l = k^{1/2}/\omega \tag{2.18}$$

2. 2. 2 $k - \epsilon$ Model:

Considering the $k - \epsilon$ model, we can refer to the equation defining the turbulence model as follows:

1. Kinematic Eddy Viscosity:

$$v_T = C_\mu k^2/\epsilon \tag{2.19}$$

2. Turbulence Kinetic Energy:

$$\frac{\partial k}{\partial t} + U_j \frac{\partial k}{\partial x_j} = \tau_{ij}\frac{\partial U_i}{\partial x_j} - \epsilon + \frac{\partial}{\partial x_j}\left[\left(v + v_T/\sigma_\epsilon\right)\frac{\partial k}{\partial x_j}\right] \tag{2.20}$$

3. Specific Dissipation Rate:

$$\frac{\partial \epsilon}{\partial t} + U_j \frac{\partial \epsilon}{\partial x_j} = C_{\epsilon 1}\frac{\epsilon}{k}\tau_{ij}\frac{\partial U_i}{\partial x_j} - C_{\epsilon 2}\frac{\epsilon^2}{k} + \frac{\partial}{\partial x_j}\left[\left(v + v_T/\sigma_\epsilon\right)\frac{\partial k}{\partial x_j}\right] \tag{2.21}$$

4. Closure Coefficients and Auxiliary Relations:

$$C_{\epsilon 1} = 1.44 \tag{2.22}$$

$$C_{\epsilon 2} = 1.92 \tag{2.23}$$

$$C_\mu = 0.09 \tag{2.24}$$

$$\sigma_k = 1.0 \tag{2.25}$$

$$\sigma_\epsilon = 1.3 \tag{2.26}$$

$$\omega = \epsilon / C_\mu k \tag{2.27}$$

$$l = C_\mu k^{3/2} / \epsilon \tag{2.28}$$

2. 2. 3 Perturbation Analysis:

The perturbation analysis of the model develops an approximate solution by including the variables in terms of small parameters. This method is useful for separately analyzing the inner and outer wall regions in the turbulent boundary layers. The log layer is an overlap region between the viscous sublayer and the defect layer, and in the defect layer, the velocity deviates slightly from the free-stream velocity.

The $k - \omega$ model uniquely handles the log and viscous sublayer without requiring empirical damping functions. Furthermore, modifications like stress limiters and cross-diffusion terms improve predictions in adverse pressure gradients and curved surfaces.

The $k - \epsilon$ model suits free-shear flows and high Reynolds number boundary layers but struggles in viscous sublayers. This results in the model needing wall-damping functions to account for high dissipation rates near the walls [18].

Table 2.1- Comparison between $k - \omega$ and $k - \epsilon$ models.

Aspect	$k - \omega$	$k - \epsilon$
Near-wall Handling	Directly models the function	Requires a damping function
Free-stream Accuracy	Sensitive to freestream conditions	Better for freestream conditions
Blending Flexibility	Used near the wall	Used in outer layers

2. 2. 4 *BSL* Model:

A new baseline model was built based on the advantages of both $k - \omega$ and $k - \epsilon$ models. This model is robust near the wall region because of $k - \omega$ model and accurate near the outer boundary layer because of the $k - \epsilon$ model.

A transformed version of the $k - \epsilon$ equations introduces a cross-diffusion term in the $k - \omega$ equations, providing the necessary computation. To ensure a smooth transition between the boundaries of the model, a blending function is used.

$$F_1 = \tanh\left(\Phi_1^4\right) \tag{2.29}$$

$$\Phi_1 = \min\left[\max\left(\frac{\sqrt{k}}{0.09\omega y}, \frac{500\mu}{\rho y^2 \omega}\right), \frac{4\rho k}{\sigma_{\omega,2} D_\omega^+ y^2}\right] \tag{2.30}$$

2. 2. 5 *SST* Model:

The shear stress transport model incorporates the modified eddy-viscosity definition to account for the shear stress transport accurately:

$$v_t = a_1 \frac{k}{\max\left(a_1\omega, SF_2\right)} \tag{2.31}$$

$$F_2 = \tanh\left[\left(\frac{2k}{\omega k}\right)^2\right] \tag{2.32}$$

The SST model improves the sensitivity of the model to adverse pressure gradient conditions. This ensures the scaling of the turbulent shear stress in boundary layers with strong viscous-inviscid interactions. Similar to the *BSL* Model, the blending function F_2 is implemented to enhance the accuracy in mixed-flow regions.

2. 2. 6 Boundary Conditions for *BSL* and *SST* Model:

1. Inlet Boundary:

- Turbulence Intensity (I) and length scale (L) are specified:

$$I = \frac{\sqrt{2k/3}}{U_\infty}, \quad L \sim 0.07\, L_c \tag{2.33}$$

2. Wall Boundary:

- No-slip condition for velocity.
- The dissipation rate ensures proper near-wall behavior.

$$\omega = \frac{10v}{\beta^* y^2} \tag{2.34}$$

3. Outlet Boundary:

- Free stream pressure and turbulence values are extrapolated.

3. Computational Setup

3.1 Finite Volume Method:

The finite volume method is used in numerical techniques for solving conservation laws in fluid mechanics, heat transfer, etc. The process is focused on a balanced approach at the control volume level. FVM is based on an integral form of conservation laws, which are discretized over control volumes:

- Local Conservation: balanced fluxes over the control volume.
- Adaptability or Arbitrary Geometry: suitable for complex and unstructured meshes.
- Robustness: handles discontinuities, which is important for shock and turbulence.

The governing equations are integrated over each control volume. Eg.

$$\frac{\partial q}{\partial t} + \nabla \cdot F = S, \tag{3.1}$$

Where q is the conserved variable, F represents the flux, and S is the source term.

Numerical implementation:

- Temporal Discretization: Time-dependent using Euler or implicit methods.
- Spatial Discretization: Surface integrals using numerical approximations.
- Boundary Conditions: To ensure continuity and conservation at the boundary and surrounding cells.

The local conservation framework makes FVM ideal for simulations of compressible and turbulent flows, such as those encountered in rocket engines [23].

3.2 Accuracy and Errors:

3. 2. 1 Truncation Error:

- Truncation errors arise due to the discretization of continuous equations. Higher-order schemes reduce truncation error but require more computational resources.

3. 2. 2 Round-off Error:

- Round-off errors occur due to machine precision limits and can be significant for large-scale simulations.

3. 2. 3 Grid Dependency:

- Accuracy depends on mesh resolution. Key strategies include:
- Ensuring near walls for boundary layer resolution.

- Refining the mesh in shock and plume interaction zones.

3.3 Assumptions:

3. 3. 1 Flow Behavior:

- Compressible flow with ideal gas behavior.

3. 3. 2 Turbulence Modeling:

- SST turbulence model, along with BSL for comparison.

3. 3. 3 Geometry Simplifications:

- Axisymmetric or symmetric configurations are assumed for computation efficiency.

3.4 Stability Considerations:

3. 4. 1 CFL Condition:

The Courant-Friedrichs-Lewy (CFL) condition governs stability for explicit time-stepping schemes:

Where:

- Time step.
- Spatial step size.
- Velocity magnitude.

3. 4. 2 Convergence Criteria:

Residuals for mass, momentum, and energy equations must drop.

3. 4. 3 Iterative Solvers:

- SIMPLE: Used for pressure-velocity coupling in steady-state simulations.
- PISO: Used for transient simulations to handle time-dependent phenomena.

3.5 Implementation of CAD Software:

3. 5. 1 CAD Modeling of Laval Nozzle and Rocket Base:

The Laval Nozzle was built on a version studied by NASA. The nozzle characteristics are well documented, and a plethora of experimental data is available, making it a suitable option for the project. Its shape, with the convergent-divergent profile, optimizes pressure recovery and reduces flow separation, making it ideal for high-thrust applications. Using the Laval Nozzle ensures efficient propulsion and precise control of exhaust plumes. The table below shows the general geometry of the nozzle used.

Table 3.1- Geometry and Configuration of the Engine.

Geometry	Value
Base Diameter, D_b	12 inches
Nozzle exit diameter, D_e	2.94 inches
Nozzle spacing ratio, D_s/D_e	1.67, 2.18, 2.5
Nozzle extension ratio, L/D_e	0.7017, 1.7326
Nozzle area ratio	12

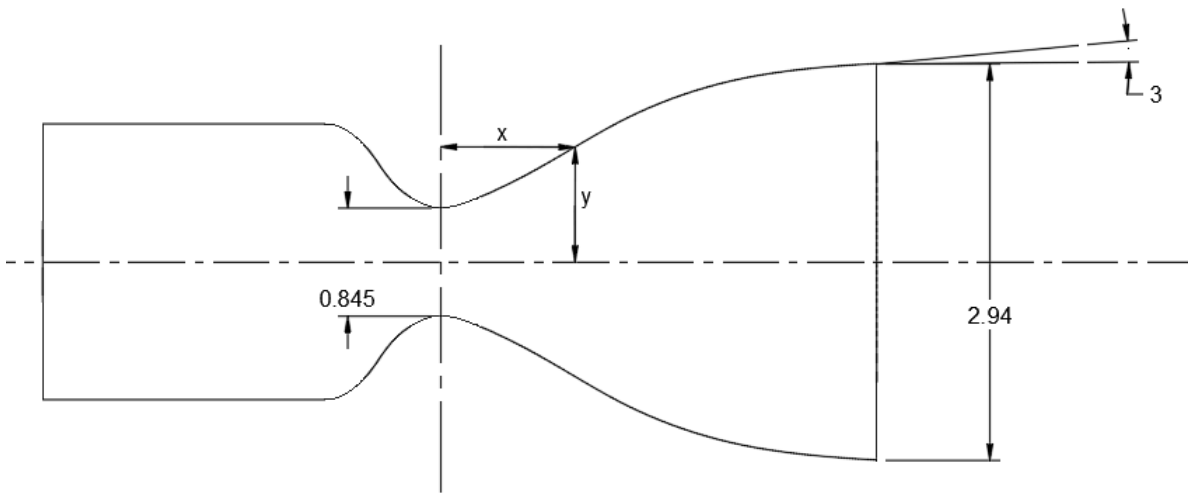

Figure 3.1- Laval Nozzle

Table 3.2- Co-ordinate for Laval Nozzle.

x, inches	y, inches
0	0.4275
0.5	0.642
1.0	0.930

1.5	1.175
2.0	1.334
2.5	1.420
3.12	1.475

3. 5. 2 Software Tools:

The nozzle geometry was created using Fusion 360 for precision and control over the contour of the nozzle. The parametric modeling feature allowed for quick changes and various nozzle configurations. The models were exported in STEP format for ANSYS Fluent meshing and simulation.

3. 5. 3 Nozzle Configurations:

1. Linear Arrangement:

Nozzles are aligned in a single row, minimizing the interaction but increasing the base area exposure to heat flux generated during ascent.

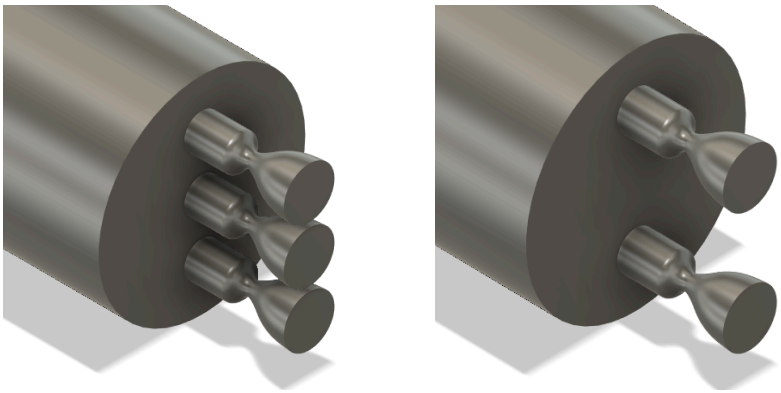

Figure 3.2- Linear Nozzles

2. Circular Arrangement:

Engines are arranged symmetrically around a central axis to optimize thrust balance.

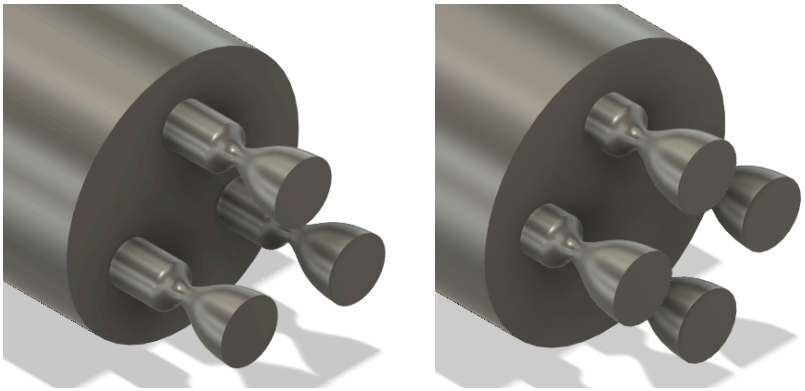

Figure 3.3- Circular Nozzles

3. Staggered Arrangement:

Engines staggered to reduce direct plume impingement on the base plate.

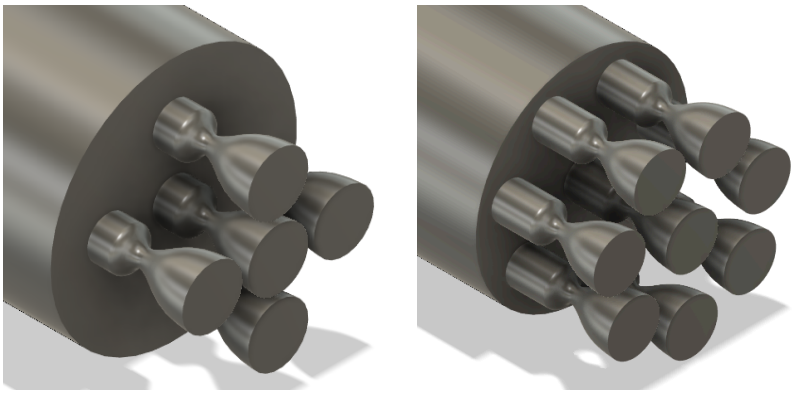

Figure 3.4- Circular Nozzles

3.6 Meshing:

3. 6. 1 Structured Grids: Structured grids were applied near nozzle walls to resolve boundary layers and minimize numerical diffusion accurately.

3. 6. 2 Unstructured Grids: Unstructured grids were used in the plume interaction and recirculation regions to handle complex geometries and interactions.

3. 6. 3 Inflation Layers: Inflation layers were added to capture near-wall effects, ensuring that for accurate boundary layer modeling.

3. 6. 4 Meshing Parameters:

1. Mesh Growth Rate:

- Value: 1.1

- A lower growth rate ensures smooth transitions between adjacent cell sizes, which is particularly useful in capturing boundary layers and regions with high gradients.

2. Mesh Target Skewness:

- Value: 0.85

- Ensures cells remain within an acceptable skewness range, reducing numerical errors and improving simulation stability.

3. Mesh Element Size:

- Value: 0.005 m

- Provides a base element size, ensuring sufficient resolution near-critical regions such as nozzle throats and plume interaction zones.

4. Mesh Max Size:

- Value: 0.02 m

- Sets an upper limit for element size in the far-field region to balance computational cost with accuracy.

5. Mesh Proximity Minimum Size:

- Value: 0.0005 m

- Ensures a finer mesh in regions where surfaces are close, such as between nozzle walls and plume boundaries.

6. Mesh Curvature Normal Angle:

- Value: 5 degrees

- Improves mesh refinement around curved geometries like nozzle contours, capturing flow behavior more accurately.

7. Mesh Maximum Layers:

- Value: 20

- Provides detailed resolution for the boundary layer, essential for accurately modeling heat flux and turbulence near walls.

These parameters were optimized to maintain a balance between computational efficiency and the resolution required for capturing key flow features, such as recirculation zones and shock structures.

1	ID	Parameter Name	Value	Unit
2	Input Parameters			
3	Fluid Flow (Fluent) (A1)			
4	P2	Mesh Growth Rate	1.1	
5	P6	Mesh Target Skewness	0.85	
6	P8	Mesh Element Size	0.005	m
7	P9	Mesh Max Size	0.02	m
8	P10	Mesh Proximity Min Size	0.0005	m
9	P11	Mesh Curvature Normal Angle	5	degree
10	P12	Mesh Maximum Layers	20	

Figure 3.5- ANSYS Parameters

8. Inflation Layers:

- y^+ goal: For the SST k–ω model, we target a first‑cell $y^+ \lesssim 1$.
- First‑layer thickness (Δ_1):

$$\Delta_1 = \frac{y^+ \nu_\infty}{u_r} \tag{3.2}$$

- where $u_r = \sqrt{\frac{\tau_\omega}{\rho_\omega}}$
- Layers: 10-20 inflation layers.
- Growth Ratio: 1.1-1.2 per layer for smooth transition of the mesh.

9. Global Face Sizing:

- To resolve the exterior shear and shock structures, enforce a maximum surface element size of De/20.

$$L_{max} = \frac{D_e}{20} \tag{3.3}$$

These parameters were optimized to maintain a balance between computational efficiency and the resolution required for capturing key flow features, such as recirculation zones and shock structures. By combining inflation and face meshing, I was able to ensure both boundary layer and large-scale lume are adequately captured without over-refining the entire domain, which also helped for faster computation.

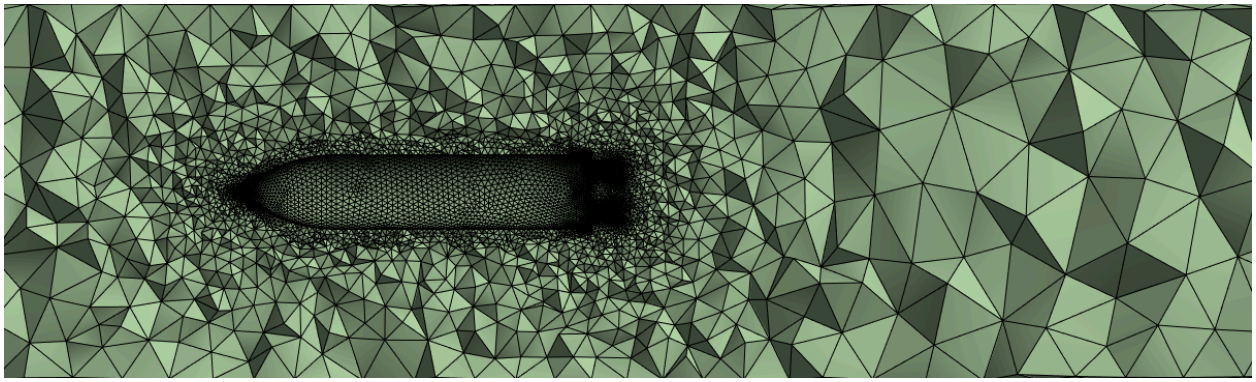

Figure 3.6- Refined mesh around the rocket and nozzles.

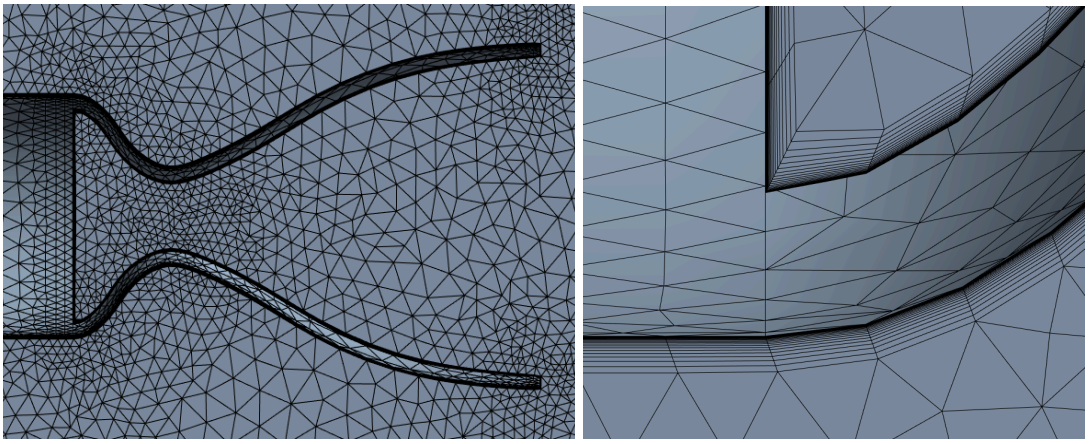

A. Refined mesh using face meshing *B. Inflation layers near the boundary*

Figure 3.7- Nozzle Meshing.

3.7 NASA CEA:

3. 7. 1 NASA CEARUN:

Developed by NASA, was used to compute equilibrium thermodynamic and transport properties of combustion for RP-1 and LOX mixture. In this, CEA 2.2 B was implemented to to generate the stagnation‑point temperature, pressure, density, species composition, and transport coefficients (viscosity, thermal conductivity) of an RP-1/LOX exhaust at our design chamber pressures. These data form the inlet boundary conditions for our ANSYS Fluent simulations, ensuring that the high-temperature, multi‑species nature of the plume is faithfully represented in the CFD domain.

3. 7. 2 Inputs:

Table 3.3- CEARUN Inputs

Input Parameter	Specification

Problem Type	Rocket (Infinite Area Combustor)
Pressure (bar)	Min: 1 Bar, Max: 12 Bar, Increment: 1 Bar
Supersonic Area Ratio (Ae/At)	12
O/F Ratio	2.2
Fuel	RP-1 (100 wt%)
Oxidizer	LOX (100 wt%)
Output Proportions	Mass Fractions
Units	SI
Transport Properties	Calculated

3. 7. 3 Setting Species Transport in Ansys:

Using the thermodynamic properties obtained from the output file, a new mixture was defined in the materials panel of ANSYS Fluent. This enabled the setup of species and the properties of the mixture to capture the thermal characteristics of the exhaust plumes with more accuracy.

3.8 Ansys Fluent Setup:

3. 8. 1 Flow Behavior:

- Compressible, steady-transient (depending on requirement), multi-species flow treated as an ideal-gas mixture.

3. 8. 2 Turbulence Modeling:

- Primary: SST $k - \omega$ RANS

3. 8. 3 Species and Chemistry:

- Mixture-species transport with 17-reaction Chemkin mechanism imported from NASA CEA.

3. 8. 4 Radiation:

- Discrete Ordinates (DO) model, grey gas assumption, with absorption/scattering coefficients from NASA CEA.

3. 8. 5 Boundary Conditions:

- Nozzle Inlets: Total Pressure P and T from CEA, mass fraction composition.
- Far-field: Ambient conditions.

- Walls/Baseplate: no-slip, base-plate and rocket records surface heat-flux, rest adiabatic.

3. 8. 6 Solver Settings:

- Density-based, implicit, double precision.
- Discretization: 1st order upwind for initial testing, then 2nd order upwind for final results.
- Under-relaxation: $k - \omega = 0.2 - 0.7$

3. 8. 7 Convergence:

- Residuals: continuity, momentum, energy, species < 1×10^{-5}; radiation < 1×10^{-6}.

4. Results and Discussions

4.1 Overview of Cases and Metrics:

To isolate the effects of nozzle count and altitude on base-heating, it was necessary to build all 3-D models and mesh them on the same parameters. After that, 2 distinct altitudes were considered, one that provides a fully expanded flow at 15240m and the other at an underexpanded flow at 30480m. Table 4.1 summarizes the various configurations used for simulations.

Table 4.1- CEARUN Inputs

Case ID	Nozzles	Altitude	Ambient Pressure	Ambient Temperature
3N-15	3	15240	9504.4	220
4N-15	4			
5N-15	5			
7N-15	7			
3N-30	3	30480	1095.233	230
4N-30	4			
5N-30	5			
7N-30	7			

4.1. 1 Parameters for all cases:

- Chamber Pressure: 6 Bar
- Turbulence Model: SST k–ω
- Radiation Model: Discrete Ordination
- Species: Transport Species (RP-1-LOX)
- Solver: Double Precision, Density Based, Steady and Transient States with Absolute Velocity Formulation
- Far-Field Conditions: Ambient pressure, ambient temperature, Mach: 2.75
- Methods: First order upwind for initial and coarse mesh, second order for final results and finer mesh.
- Mesh: 1.2 - 1.6 million cells (y+~3.72e-6, De/20 Face Sizing)

4.2 Effects of Altitude on Base Heating:

From the contour figure 4.1, a clear trend is observed: as the rocket reaches higher altitudes, the plume interactions increase due to underexpanded flow after the exit. At low altitudes, where the flow is fully expanded, the higher ambient pressure results in more confined plumes and less interaction, and weaker recirculation zones. As the rocket ascends, the ambient pressure decreases, and the exhaust underexpands, resulting in severe impingement, causing choked recirculating base flow, leading to:

- Larger and more energetic recirculation zones.
- Formation of a central hot zone due to increased plume interaction.
- Broader distribution of high-temperature regions across the baseplate.

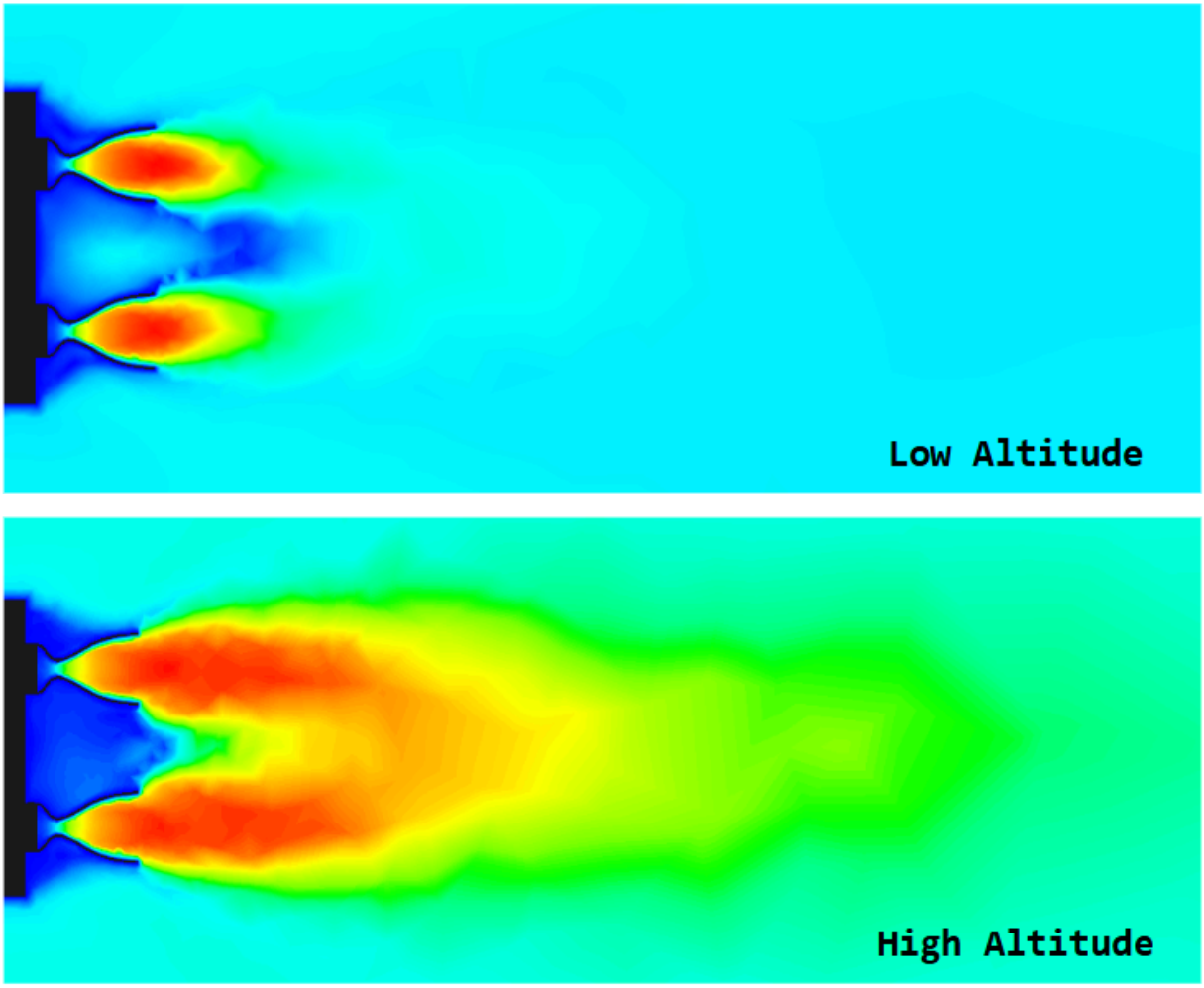

Figure 4.1- 4-Nozzle Configuration Mach Number Contours

4.3 Effects of Altitude on Base Heating:

4.3.1 Three Nozzle Configuration:

- At low altitude, heat is mainly limited to the nozzle edges; the center remains relatively cooler.
- At high altitude, increased expansion leads to stronger central heating, but the spacing reduces extreme overlap. Still, noticeable reverse flow and heat accumulation occur in the central region.

4.3.2 Four Nozzle Configuration:

- At low altitude, the thermal field is relatively balanced with moderate interaction between plumes.

- At high altitude, strong symmetrical recirculation and plume impingement lead to the highest base heating intensity among all cases. The center becomes a hot spot due to the confined geometry, encouraging plume collision.

4.3.3 Staggered Nozzle Configuration:

- As nozzle count increases, plume interactions become more complex and overlap more strongly, particularly at high altitude.

- In the seven-nozzle case, severe central heating is expected due to the tight clustering, but outer nozzles may slightly deflect the central updraft plume, depending on spacing. Thus, reducing the chances of severe heat flux at the centre of the base plate.

- Higher nozzle count can lead to more uniform base heating, but at the cost of increased complexity and structural stress on the base plate.

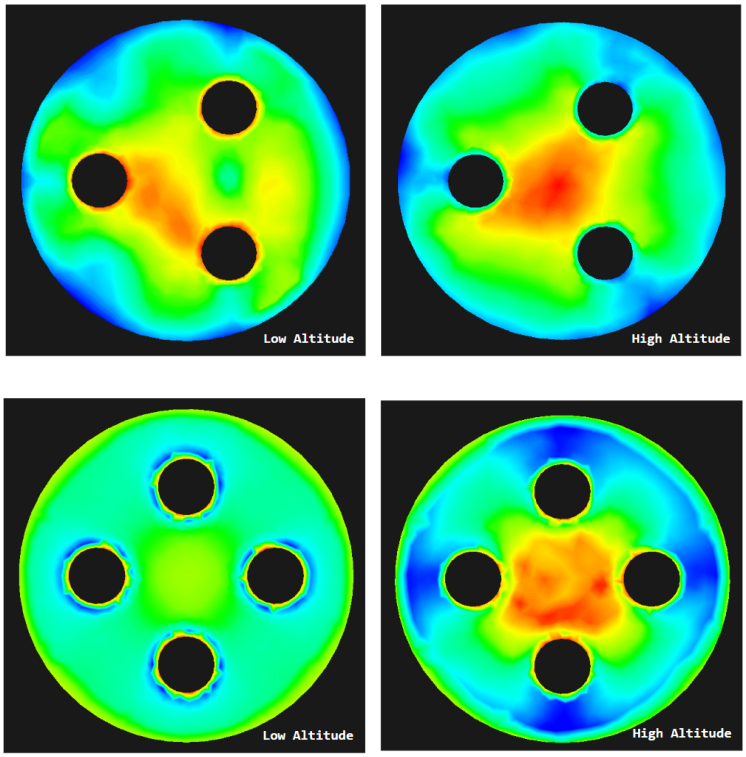

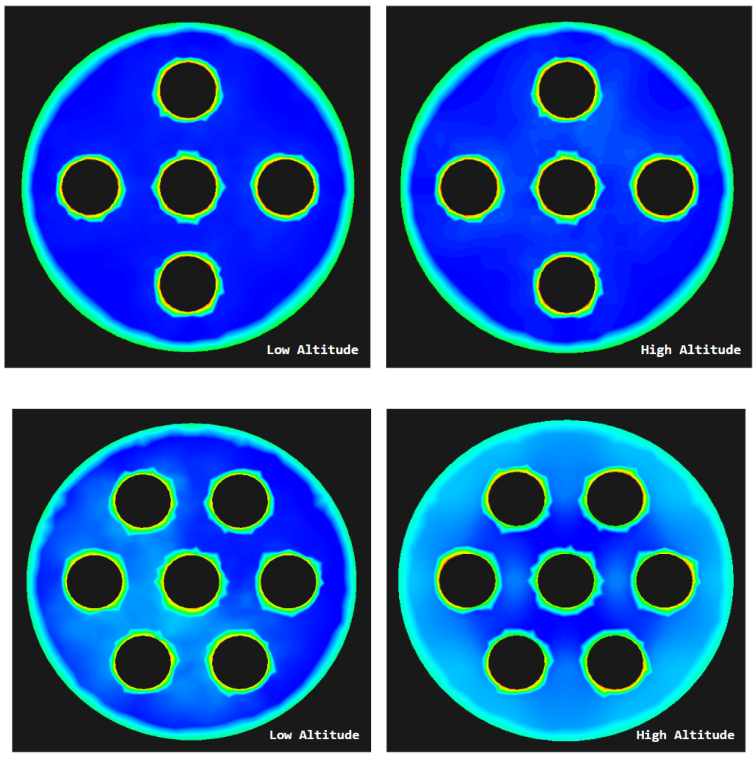

Figure 4.2- Temperature contours for nozzle configuration at low and high altitudes.

Table 4.2- Results Summary

Nozzle Configuration	Altitude	Base Flow Behavior	Central Heating	Recirculation Strength	Comment
3	Low	Mild Interaction	Low	Weak	Mild heating
3	High	Plume Overlap	Moderate	Moderate	Central zone heating
4	Low	Symmetrical, Isolated	Low	Minimal	Clean separation between plumes
4	High	Strong Interaction	Very High	Strong	Hotspot formed in the centre
7	Low	Well	Very Low	Moderate	Heating

		Separated			mostly near the nozzles
7	High	Overlapping Plumes	Low	Very Strong	Even and widespread heating

4.4 Discussions:

4.4.1 Plume Interactions:

These simulations reveal a clear trend of base heating being affected by the plume interactions across all nozzle configurations. At low altitudes, higher ambient pressure results in isolated plumes, which do not interact with each other and cause weaker recirculation of exhaust gases. As the plume is underexpanded due to the decreasing ambient pressure, the exhaust from each nozzle impinges on the neighbouring nozzles to generate large recirculation zones, shock convergence, and hot updraft plumes near the base region. Thus, nozzle design should accommodate these considerations, as a high plume ratio (P_e/P_∞) causes the jets to spread outwards and interact strongly.

4.4.2 Observations:

These observations are consistent with the studies carried out in Zhou et al. [2023], where base heat flux is increased by over 50% when transitioning from a three-nozzle to four-nozzle configuration. Furthermore, nozzle clustering affects the thermal behavior of the base region. Four-nozzle configuration case shows the highest heat concentration at the centre of the base plate during high altitude, a result of shock-shock interactions and stagnation of the updraft flow.

4.4.3 Turbulence Effects:

Turbulence plays a key role in base region heating. The mixing and recirculation of hot exhaust gases increase the local turbulence, causing convective heat transfer in the region. When species transport was modeled, additional heating resulted in a higher temperature rise on the base plate.

4.4.4 Design Considerations:

- Strong central heating in high nozzle-count configurations demands robust thermal protection systems (TPS), particularly for base electronics and structural supports.

- The added mass of TPS due to poor thermal layouts could reduce payload capacity.

- Staggered nozzle arrangements may reduce central heating and offer a better thermal load distribution.

5. Conclusions and Future Work

This study focused on understanding the base flow characteristics and thermal environment of multi-nozzle clustered rocket configurations using CFD simulations in ANSYS Fluent. The aim was to evaluate how the number of nozzles and flight altitude impact base heating, recirculation, and plume interaction patterns.

From the results, a clear trend was observed — base heating increases with altitude. This is because at higher altitudes, the ambient pressure drops, causing the exhaust to become underexpanded. This leads to stronger plume interactions, formation of central recirculation zones, and higher temperature regions on the baseplate. Among all the configurations, the four-nozzle and seven-nozzle setups showed the highest central heating due to symmetric plume collisions and strong updraft flow.

It was also observed that staggered nozzle configurations reduce the central heating by breaking the symmetry, they deflect the recirculating plume outward, and reduce direct impact. This is one of the reasons why newer rockets like Falcon-9 use radial or staggered nozzle layouts, effectively reducing thermal load on base plate structures. Even the Saturn-V first stage used a 5-nozzle configuration during the Apollo Missions.

These simulations show the impact of nozzle placement and altitude on the base plate and the region around it. It is necessary to address these issues in newer rocket designs, as these rockets usually opt for multi-nozzle configurations. These studies can provide insight into the factors affecting the base region and the ways of mitigating thermal load during ascent.

While the results matched the expectations and available literature, there are a few things that can be improved:

- A finer mesh can provide better estimation of the properties and help improve the accuracy of the model. This includes increasing the inflation layers and capturing more of the surroundings for plume interactions.
- Turbulence Modeling can be improved using LES or hybrid RAN-LES models that are better at capturing the unsteady flows and their interactions, but were left out of the study due to computational limits.
- The Radiation model assumed a grey gas, this can be replaced with an actual spectral model for high-temperature radiative heat transfer.
- Further work on the placement of nozzles and finding the optimum empirical relations can help balance performance and base heating.
- Finally, considering a full thermodynamic model for the exhaust gases for more accurate thermal characterization of the plumes and base regions.

References

[1] Raje, P. V., and Sinha, K., “Three-Dimensional Simulation of Rocket Nozzles with Multi-Jet Interaction Using Shock-Unsteadiness Model,” presented at the AIAA Aviation 2019 Forum, Dallas, Texas, 2019. https://doi.org/10.2514/6.2019-3322

[2] Mehta, M., Dufrene, A. T., Seaford, M., and Knox, K., “Space Launch System Base Heating Test: Environments and Base Flow Physics,” presented at the 54th AIAA Aerospace Sciences Meeting, San Diego, California, USA, 2016. https://doi.org/10.2514/6.2016-0547

[3] Mehta, M., Canabal, F., Tashakkor, S. B., and Smith, S. D., “Numerical Base Heating Sensitivity Study for a Four-Rocket Engine Core Configuration,” *Journal of Spacecraft and Rockets*, Vol. 50, No. 3, 2013, pp. 509–526. https://doi.org/10.2514/1.A32287

[4] Nallasamyl, R., and Kandula, M., “Base Flow and Heat Transfer Characteristics of a Four-Nozzle Clustered Rocket Engine: Effect of Nozzle Pressure Ratio.”

[5] Wang, X., Xu, X., and Yang, Q., “Numerical Analysis on Thermal Environment of Reusable Launch Vehicle during Supersonic Retropropulsion,” *International Journal of Thermal Sciences*, Vol. 198, 2024, p. 108857. https://doi.org/10.1016/j.ijthermalsci.2023.108857

[6] Ebrahimi, H. B., Levine, J., and Kawasaki, A., “Numerical Investigation of Twin-Nozzle Rocket Plume Phenomenology.”

[7] Musial, N., and Ward, J., “Base Flow Characteristics for Several Four-Clustered Rocket Configurations at Mach Numbers from 2.0 to 3.5.,” 1961, p. 54.

[8] Zhou, Z., Liang, X., Zhao, C., Le, G., and Ding, Y., “Investigations of Base Thermal Environment on Four-Nozzle Liquid Launch Vehicle at High Altitude,” *Journal of Spacecraft and Rockets*, Vol. 57, No. 1, 2020, pp. 49–57. https://doi.org/10.2514/1.A34492

[9] Пилипенко, О., Долгополов, С., Ніколаєв, О., Хоряк, Н., Кваша, Ю., and Башлій, І., “ВИЗНАЧЕННЯ РОЗКИДУ ТЯГИ БАГАТОДВИГУННОЇ УСТАНОВКИ І СТУПЕНЯ РАКЕТИ-НОСІЯ «ЦИКЛОН-4М» ПРИ ЇЇ ЗАПУСКУ,” *Science and Innovation*, Vol. 18, No. 6, 2022, pp. 97–112. https://doi.org/10.15407/scine18.06.097

[10] Dolgopolov, S. I., Nikolayev, O. D., and Khoriak, N. V., “Dynamic Interaction between Clustered Liquid Propellant Rocket Engines under Their Asynchronous Start-Ups,” *Propulsion and Power Research*, Vol. 10, No. 4, 2021, pp. 347–359. https://doi.org/10.1016/j.jppr.2021.12.001

[11] Долгополов, С., “УЗАГАЛЬНЕННЯ ЕКСПЕРИМЕНТАЛЬНОЇ ПРУЖНОСТІ КАВІТАЦІЙНИХ КАВЕРН У НАСОСАХ РРД, ЯКІ ІСТОТНО ВІДРІЗНЯЮТЬСЯ ЗА РОЗМІРАМИ ТА ПРОДУКТИВНІСТЮ,” *Science and Innovation*, Vol. 19, No. 5, 2023, pp. 71–88. https://doi.org/10.15407/scine19.05.071

[12] Wang, T., Ding, Q., Tang, Y., and Ma, Z.-S., “Enhanced Method for Analyzing Pogo Stability of Liquid Rockets with Uncertain-But-Bounded Parameters,” *Journal of Spacecraft and Rockets*, Vol. 59, No. 3, 2022, pp. 728–738. https://doi.org/10.2514/1.A35064

[13] Dolgopolov, S., and Nikolayev, O., “Features of Mathematical Modeling of Nonlinear Pogo Oscillations of Launch Vehicles,” *CEAS Space Journal*, Vol. 16, No. 6, 2024, pp. 699–713. https://doi.org/10.1007/s12567-024-00541-3

[14] Pu, P., and Jiang, Y., “Assessing Turbulence Models on the Simulation of Launch Vehicle Base Heating,” *International Journal of Aerospace Engineering*, Vol. 2019, 2019, pp. 1–14.

https://doi.org/10.1155/2019/4240980
[15] Spalart, P., and Allmaras, S., “A One-Equation Turbulence Model for Aerodynamic Flows,” presented at the 30th Aerospace Sciences Meeting and Exhibit, Reno,NV,U.S.A., 1992. https://doi.org/10.2514/6.1992-439
[16] Shih, T.-H., Liou, W. W., Shabbir, A., Yang, Z., and Zhu, J., “A New K-ϵ Eddy Viscosity Model for High Reynolds Number Turbulent Flows,” *Computers & Fluids*, Vol. 24, No. 3, 1995, pp. 227–238. https://doi.org/10.1016/0045-7930(94)00032-T
[17] Yakhot, V., “Renormalization Group for Modelling of Turbulent Flows and Turbulentcombustion,” presented at the 29th Aerospace Sciences Meeting, Reno,NV,U.S.A., 1991. https://doi.org/10.2514/6.1991-218
[18] Menter, F. R., “Two-Equation Eddy-Viscosity Turbulence Models for Engineering Applications,” *AIAA Journal*, Vol. 32, No. 8, 1994, pp. 1598–1605. https://doi.org/10.2514/3.12149
[19] Menter, F. R., Kuntz, M., and Langtry, R., “Ten Years of Industrial Experience with the SST Turbulence Model,” *Heat and Mass Transfer*.
[20] “2006_Wilcox_Turbulence-Modeling-for-CFD.Pdf.”
[21] Sinha, K., Mahesh, K., and Candler, G., “Modeling the Effect of Shock Unsteadiness in Shock-Wave / Turbulent Boundary Layer Interactions,” presented at the 42nd AIAA Aerospace Sciences Meeting and Exhibit, Reno, Nevada, 2004. https://doi.org/10.2514/6.2004-1129
[22] Zhou, Z., and Bao, Y., “Investigating the Rocket Base Flow Characteristics and Thermal Environment of Different Nozzle Configurations Considering Afterburning,” *International Journal of Thermal Sciences*, Vol. 185, 2023, p. 108073. https://doi.org/10.1016/j.ijthermalsci.2022.108073
[23] Eymard, R., Gallouët, T., and Herbin, R., “Finite Volume Methods.”

Appendix A: NASA CEARUN Input File

```
### CEA analysis performed on Tue 06-April-2025 01:37:02
# Problem Type: "Rocket" (Infinite Area Combustor)
prob case = _________________4057 ro equilibrium
# Pressure (12 values):
p,bar= 1, 2, 3, 4, 5, 6, 7, 8, 9, 10, 11, 12
# Supersonic Area Ratio (1 value):
supar= 12
# Oxidizer/Fuel Wt. ratio (1 value):
o/f = 2.2
# You selected the following fuels and oxidizers:
reac
fuel RP-1              wt%=100.0000
oxid O2(L)             wt%=100.0000
# You selected these options for output:
# long version of output
# Proportions of any products will be expressed as Mass Fractions.
output massf
# Heat will be expressed as siunits
output siunits
# Transport properties calculated
output transport
# Plot parameters:
output plot p t rho cp h u mach aeat
# Input prepared by this script:/var/www/sites/cearun/cgi-bin/CEARUN/prepareInputFile.cgi
### IMPORTANT:  The following line is the end of your CEA input file!
end
```

Appendix B: NASA CEARUN Output File

```
*****************************************************************

NASA-GLENN CHEMICAL EQUILIBRIUM PROGRAM CEA2, FEBRUARY 5, 2004

            BY  BONNIE MCBRIDE AND SANFORD GORDON

REFS:    NASA  RP-1311,  PART  I,  1994  AND  NASA  RP-1311,  PART  II,  1996
         *********************************************************************

OPTIONS: TP=F  HP=F  SP=F  TV=F  UV=F  SV=F  DETN=F  SHOCK=F  REFL=F  INCD=F

 RKT=T  FROZ=F  EQL=T  IONS=F  SIUNIT=T  DEBUGF=F  SHKDBG=F  DETDBG=F  TRNSPT=T

 TRACE= 0.00E+00  S/R= 0.000000E+00  H/R= 0.000000E+00  U/R= 0.000000E+00

 Pc, BAR =     1.000000     2.000000     3.000000     4.000000     5.000000     6.000000     7.000000

 Pc ,BAR =     8.000000     9.000000    10.000000    11.000000    12.000000

 Pc/P =

 SUBSONIC AREA RATIOS =

 SUPERSONIC AREA RATIOS =    12.0000

 NFZ=  1  Mdot/Ac= 0.000000E+00  Ac/At= 0.000000E+00

   REACTANT         WT.FRAC   (ENERGY/R), K   TEMP ,K  DENSITY

      EXPLODED FORMULA

 F: RP-1            1.000000  -0.297284E+04   298.15  0.0000

       C  1.00000  H  1.95000

 O: O2(L)           1.000000  -0.156101E+04    90.00  0.0000

       O  2.00000

  SPECIES BEING CONSIDERED IN THIS SYSTEM

 (CONDENSED PHASE MAY HAVE NAME LISTED SEVERAL TIMES)

  LAST thermo.inp UPDATE:    9/09/04

  g 7/97  *C             tpis79  *CH            g 4/02  CH2

  g 4/02  CH3             g11/00  CH2OH          g 7/00  CH3O

  g 8/99  CH4             g 7/00  CH3OH          srd 01  CH3OOH

  tpis79  *CO             g 9/99  *CO2           tpis91  COOH

  tpis91  *C2             g 6/01  C2H            g 1/91  C2H2,acetylene
```

g 5/01 C2H2,vinylidene g 4/02 CH2CO,ketene g 3/02 O(CH)2O

srd 01 HO(CO)2OH g 7/01 C2H3,vinyl g 6/96 CH3CO,acetyl

g 1/00 C2H4 g 8/88 C2H4O,ethylen-o g 8/88 CH3CHO,ethanal

g 6/00 CH3COOH srd 01 OHCH2COOH g 7/00 C2H5

g 7/00 C2H6 g 8/88 C2H5OH g 7/00 CH3OCH3

srd 01 CH3O2CH3 g 8/00 C2O tpis79 *C3

n 4/98 C3H3,1-propynl n 4/98 C3H3,2-propynl g 2/00 C3H4,allene

g 1/00 C3H4,propyne g 5/90 C3H4,cyclo- g 3/01 C3H5,allyl

g 2/00 C3H6,propylene g 1/00 C3H6,cyclo- g 6/01 C3H6O,propylox

g 6/97 C3H6O,acetone g 1/02 C3H6O,propanal g 7/01 C3H7,n-propyl

g 9/85 C3H7,i-propyl g 2/00 C3H8 g 2/00 C3H8O,1propanol

g 2/00 C3H8O,2propanol g 7/88 C3O2 g tpis *C4

g 7/01 C4H2,butadiyne g 8/00 C4H4,1,3-cyclo- n10/92 C4H6,butadiene

n10/93 C4H6,1butyne n10/93 C4H6,2butyne g 8/00 C4H6,cyclo-

n 4/88 C4H8,1-butene n 4/88 C4H8,cis2-buten n 4/88 C4H8,tr2-butene

n 4/88 C4H8,isobutene g 8/00 C4H8,cyclo- g10/00 (CH3COOH)2

n10/84 C4H9,n-butyl n10/84 C4H9,i-butyl g 1/93 C4H9,s-butyl

g 1/93 C4H9,t-butyl g12/00 C4H10,n-butane g 8/00 C4H10,isobutane

g 8/00 *C5 g 5/90 C5H6,1,3cyclo- g 1/93 C5H8,cyclo-

n 4/87 C5H10,1-pentene g 2/01 C5H10,cyclo- n10/84 C5H11,pentyl

g 1/93 C5H11,t-pentyl n10/85 C5H12,n-pentane n10/85 C5H12,i-pentane

n10/85 CH3C(CH3)2CH3 g 2/93 C6H2 g11/00 C6H5,phenyl

g 8/00 C6H5O,phenoxy g 8/00 C6H6 g 8/00 C6H5OH,phenol

g 1/93 C6H10,cyclo- n 4/87 C6H12,1-hexene g 6/90 C6H12,cyclo-

n10/83 C6H13,n-hexyl g 6/01 C6H14,n-hexane g 7/01 C7H7,benzyl

g 1/93 C7H8 g12/00 C7H8O,cresol-mx n 4/87 C7H14,1-heptene

n10/83 C7H15,n-heptyl n10/85 C7H16,n-heptane n10/85 C7H16,2-methylh

n 4/89 C8H8,styrene n10/86 C8H10,ethylbenz n 4/87 C8H16,1-octene

n10/83 C8H17,n-octyl n 4/85 C8H18,n-octane n 4/85 C8H18,isooctane

n10/83 C9H19,n-nonyl g 3/01 C10H8,naphthale n10/83 C10H21,n-decyl

G12/12 C11H21 g 8/00 C12H9,o-bipheny g 8/00 C12H10,biphenyl

g 6/97 *H g 1/01 HCO g 6/01 HCCO

g 4/02 HO2 tpis78 *H2 g 5/01 HCHO,formaldehy

g 6/01 HCOOH g 8/89 H2O g 6/99 H2O2

g 6/01 (HCOOH)2 g 5/97 *O g 4/02 *OH

tpis89 *O2 g 8/01 O3 g 12/0 THDCPD,endo

g 12/0 THDCPD,exo n 4/83 C(gr) n 4/83 C(gr)

n 4/83 C(gr) n12/84 CH3OH(L) n12/84 C2H5OH(L)

n 4/85 C6H14(L),n-hexa n10/86 C6H6(L) g11/99 H2O(cr)

g 8/01 H2O(L) g 8/01 H2O(L)

SPECIES WITH TRANSPORT PROPERTIES

PURE SPECIES

BINARY INTERACTIONS

O/F = 2.200000

	EFFECTIVE FUEL	EFFECTIVE OXIDANT	MIXTURE
ENTHALPY	h(2)/R	h(1)/R	h0/R
(KG-MOL)(K)/KG	-0.21270751E+03	-0.48783267E+02	-0.10000959E+03
KG-FORM.WT./KG	bi(2)	bi(1)	b0i
*C	0.71550294E-01	0.00000000E+00	0.22359467E-01
*H	0.13952307E+00	0.00000000E+00	0.43600960E-01
*O	0.00000000E+00	0.62502344E-01	0.42970361E-01

POINT ITN T C H O

Pinf/Pt = 1.724371

Pinf/Pt = 1.723633

THEORETICAL ROCKET PERFORMANCE ASSUMING EQUILIBRIUM

COMPOSITION DURING EXPANSION FROM INFINITE AREA COMBUSTOR

Pin = 87.0 PSIA

CASE = _____

REACTANT	WT FRACTION	ENERGY	TEMP

(SEE NOTE) KJ/KG-MOL K

FUEL RP-1 1.0000000 -24717.700 298.150

OXIDANT O2(L) 1.0000000 -12979.000 90.000

O/F= 2.20000 %FUEL= 31.250000 R,EQ.RATIO= 1.548030 PHI,EQ.RATIO= 1.548030

	CHAMBER	THROAT	EXIT
Pinf/P	1.0000	1.7320	94.470
P, BAR	6.0000	3.4642	0.06351
T, K	3240.26	3076.54	1802.94
RHO, KG/CU M	4.7500-1	2.9277-1	9.5909-3
H, KJ/KG	-831.53	-1503.18	-5177.47
U, KJ/KG	-2094.70	-2686.42	-5839.68
G, KJ/KG	-41639.3	-40249.0	-27883.7
S, KJ/(KG)(K)	12.5940	12.5940	12.5940
M, (1/n)	21.328	21.618	22.637
(dLV/dLP)t	-1.03312	-1.02591	-1.00018
(dLV/dLT)p	1.6279	1.5171	1.0054
Cp, KJ/(KG)(K)	6.7854	6.1027	2.0594
GAMMAs	1.1352	1.1353	1.2197
SON VEL, M/SEC	1197.5	1159.0	898.7
MACH NUMBER	0.000	1.000	3.280

TRANSPORT PROPERTIES (GASES ONLY)

CONDUCTIVITY IN UNITS OF MILLIWATTS/(CM)(K)

VISC, MILLIPOISE	1.1030	1.0628	0.74517

WITH EQUILIBRIUM REACTIONS

Cp, KJ/(KG)(K)	6.7854	6.1027	2.0594
CONDUCTIVITY	23.5879	20.8941	3.4952
PRANDTL NUMBER	0.3173	0.3104	0.4390

WITH FROZEN REACTIONS

Cp, KJ/(KG)(K) 2.0921 2.0812 1.9268

CONDUCTIVITY 4.8453 4.5991 3.0125

PRANDTL NUMBER 0.4763 0.4809 0.4766

PERFORMANCE PARAMETERS

Ae/At 1.0000 12.000

CSTAR, M/SEC 1768.2 1768.2

CF 0.6555 1.6673

Ivac, M/SEC 2179.9 3172.8

Isp, M/SEC 1159.0 2948.2

MASS FRACTIONS

*CO 0.49828 0.49004 0.43353

*CO2 0.20112 0.21407 0.30287

COOH 0.00001 0.00000 0.00000

*H 0.00226 0.00187 0.00003

HCO 0.00001 0.00000 0.00000

HO2 0.00002 0.00001 0.00000

*H2 0.01317 0.01309 0.01625

H2O 0.23760 0.24574 0.24727

*O 0.00580 0.00377 0.00000

*OH 0.03261 0.02516 0.00006

*O2 0.00913 0.00624 0.00000

* THERMODYNAMIC PROPERTIES FITTED TO 20000.K

PRODUCTS WHICH WERE CONSIDERED BUT WHOSE MASS FRACTIONS

WERE LESS THAN 5.000000E-06 FOR ALL ASSIGNED CONDITIONS

*C *CH CH2 CH3 CH2OH

CH3O CH4 CH3OH CH3OOH *C2

C2H C2H2,acetylene C2H2,vinylidene CH2CO,ketene O(CH)2O

HO(CO)2OH C2H3,vinyl CH3CO,acetyl C2H4 C2H4O,ethylen-o

CH3CHO,ethanal CH3COOH OHCH2COOH C2H5 C2H6

C2H5OH CH3OCH3 CH3O2CH3 C2O *C3

C3H3,1-propynl C3H3,2-propynl C3H4,allene C3H4,propyne C3H4,cyclo-

C3H5,allyl C3H6,propylene C3H6,cyclo- C3H6O,propylox C3H6O,acetone

C3H6O,propanal C3H7,n-propyl C3H7,i-propyl C3H8 C3H8O,1propanol

C3H8O,2propanol C3O2 *C4 C4H2,butadiyne C4H4,1,3-cyclo-

C4H6,butadiene C4H6,1butyne C4H6,2butyne C4H6,cyclo- C4H8,1-butene

C4H8,cis2-buten C4H8,tr2-butene C4H8,isobutene C4H8,cyclo- (CH3COOH)2

C4H9,n-butyl C4H9,i-butyl C4H9,s-butyl C4H9,t-butyl C4H10,n-butane

C4H10,isobutane *C5 C5H6,1,3cyclo- C5H8,cyclo- C5H10,1-pentene

C5H10,cyclo- C5H11,pentyl C5H11,t-pentyl C5H12,n-pentane C5H12,i-pentane

CH3C(CH3)2CH3 C6H2 C6H5,phenyl C6H5O,phenoxy C6H6

C6H5OH,phenol C6H10,cyclo- C6H12,1-hexene C6H12,cyclo- C6H13,n-hexyl

C6H14,n-hexane C7H7,benzyl C7H8 C7H8O,cresol-mx C7H14,1-heptene

C7H15,n-heptyl C7H16,n-heptane C7H16,2-methylh C8H8,styrene C8H10,ethylbenz

C8H16,1-octene C8H17,n-octyl C8H18,n-octane C8H18,isooctane C9H19,n-nonyl

C10H8,naphthale C10H21,n-decyl C11H21 C12H9,o-bipheny C12H10,biphenyl

HCCO HCHO, formaldehyde HCOOH H2O2 (HCOOH)2

O3 THDCPD,endo THDCPD,exo C(gr) CH3OH(L)

C2H5OH(L) C6H14(L),n-hexa C6H6(L) H2O(cr) H2O(L)

NOTE. WEIGHT FRACTION OF FUEL IN TOTAL FUELS AND OF OXIDANT IN TOTAL OXIDANTS

POINT ITN T C H O

Pinf/Pt = 1.732669

Pinf/Pt = 1.732820

Above is the part of the output for 6 Bar (87 PSIA) showing the species transport and the parameters for the mixture and the expected exit Mach, which was verified by the output in ANSYS Fluent.